RSC Advances

This is an *Accepted Manuscript*, which has been through the Royal Society of Chemistry peer review process and has been accepted for publication.

Accepted Manuscripts are published online shortly after acceptance, before technical editing, formatting and proof reading. Using this free service, authors can make their results available to the community, in citable form, before we publish the edited article. This *Accepted Manuscript* will be replaced by the edited, formatted and paginated article as soon as this is available.

You can find more information about *Accepted Manuscripts* in the Information for Authors.

Please note that technical editing may introduce minor changes to the text and/or graphics, which may alter content. The journal's standard Terms & Conditions and the Ethical guidelines still apply. In no event shall the Royal Society of Chemistry be held responsible for any errors or omissions in this *Accepted Manuscript* or any consequences arising from the use of any information it contains.

ROYAL SOCIETY OF CHEMISTRY

www.rsc.org/advances

Graphical Abstract

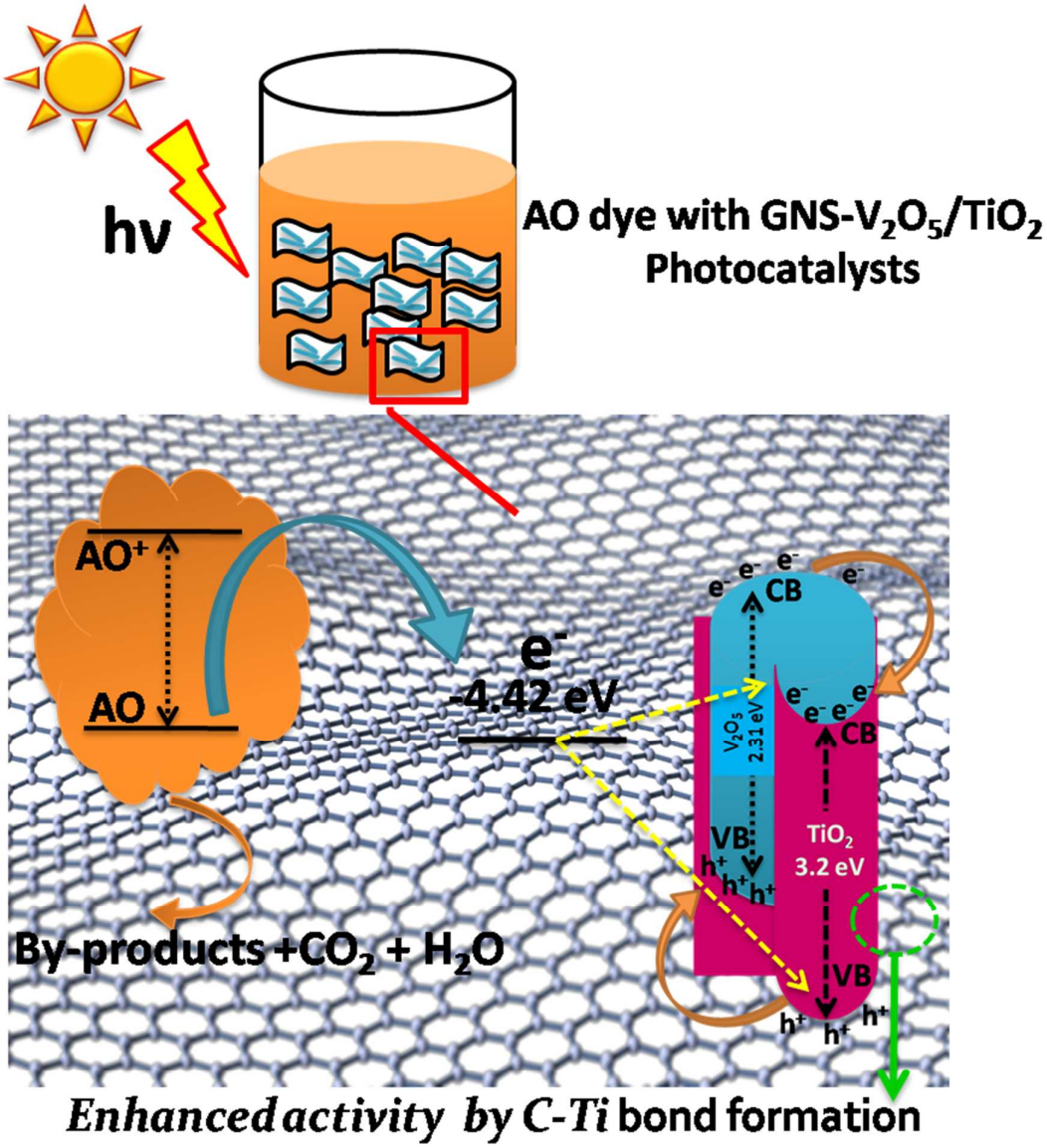

RSC Advances Accepted Manuscript

RSC Advances RSCPublishing

ARTICLE

Nanostructuring of GNS-V_2O_5/TiO_2 Core/Shell Photocatalyst for Water Remediation Applications under Sun-light Irradiation

Cite this: DOI: 10.1039/x0xx00000x

Received 00th January 2014,
Accepted 00th January 2014

DOI: 10.1039/x0xx00000x

www.rsc.org/

R. Ajay Rakkesh, D. Durgalakshmi and S. Balakumar,

The GNS-V_2O_5/TiO_2 composite, as a new class of nanoarchitecture, have been successfully fabricated by a facile hydrothermal process followed by a sol-gel technique. Such nanoarchitecture is made up of V_2O_5/TiO_2 core/shell nanorods, chemically anchored on graphene nanosheets (GNS). High-resolution scanning transmission electron microscopy shows that these core/shell nanoparticles consist of core V_2O_5 nanorods of diameter 120 nm to 140 nm, covered by TiO_2 shell of about 15 nm to 20 nm thickness. Large quantities of core/shell nanostructure materials are uniformly embedded on the surface of GNS. These new nanoarchitectures consists of two different kinds of metal oxides, that is V_2O_5 and TiO_2 which are electrostatically coupled with each other and decorated on the GNS by chemical bonding between C-Ti confirmed by Zeta potential analyzer and XPS studies, respectively. The sunlight-active photocatalytic properties of the GNS-V_2O_5/TiO_2 nanoarchitectures have been evaluated by photodegradation of acridine orange (AO) dye in an aqueous medium. Results show that the enhancement in the photocatalytic activity was attributed to the synergetic effect and also the chemical bonding leads to the interfacial charge transfer effect between GNS-semiconductor interfaces. It remarkably increases the spatial condition for charge transport and also increases the number of holes participating in the photodegradation process. This new nanoarchitecture exhibits an efficient photocatalytic activity and very high stability, holding great potential as a highly stable and reusable material for energy, water splitting, and environmental cleaning applications.

1. Introduction

Recently, the design and fabrication of core/shell nanostructures have attracted much attention due to their unique morphological-dependent properties.[1-2] The interactions between the core and shell material can drastically improve the overall performance of the core/shell nanostructure system and even create advantageous synergetic effects, which may bring a series of opportunities for their potential applications such as chemical sensors, light-emitting diodes, photocatalysis.[2-5] In particular, one-dimensional core/shell heterostructure photocatalysts have created excellent photocatalytic efficiency because of proper junctions formed between core and shell material. It can efficiently generate charge separation and the large aspect ratio can increase the active sites and wide range of light absorption.[6-8] This simple method to fabricate hierarchical core/shell nanoarchitecture is highly desirable now as well as in the near future for energy and environment cleaning applications.

Metal oxides have been broadly investigated and proven to be a group of highly efficient catalysts for photodegradation reactions. Typically, titanium dioxide (TiO_2) is a commercially available photocatalyst, because it is stable, chemically inert, inexpensive, biocompatible, and an environmentally friendly material.[9-10] The main disadvantage of TiO_2 in photocatalytic activity are, (i) wide band gap energy (3.2 eV), i.e., it can be excited only by UV light region (<390 nm), which is about 4% of the incoming solar light, whereas for commercial applications, the absorption spectrum of TiO_2 should be extended towards visible range (ii) fast electron–hole recombination. In order to avoid these limitations, many methods have been used, such as ion doping of metals and non-metals, combination with a narrow band gap semiconductor, and surface modification. A considerable enhancement in the photocatalytic efficiency of TiO_2 under visible light has been obtained by coupling low bandgap semiconductors with TiO_2.[11-12] As an important transition metal-oxide semiconductor; V_2O_5 has relatively low bandgap energy (about

RSC Advances Accepted Manuscript

2.3 eV), which can provide a capability of absorbing a broad solar spectrum.[8]

To improve the photocatalytic activity, it is highly desirable to fabricate core/shell heterostructure composite, which can efficiently promote charge separation and lead to enhanced photocatalytic activity.[13] So, the combination of V_2O_5/TiO_2 nanorods in single core/shell nanostructures could hold possible applications in energy conversion for the photodegradation reaction.[14(a-e)] Recently, graphene nanosheets (GNS) have been garnering great interest due to their superior electron mobility and high specific surface area.[15-16] By integrating GNS with V_2O_5/TiO_2 core/shell nanorods, photocatalytic activity of the semiconductors can be enhanced due to transfer of photogenerated electrons from the semiconductor to the GNS, and inhibit the recombination rate by developing local internal electric field at the interface of the heterojunction.[17-18] Further studies reveal that the interaction between GNS-V_2O_5/TiO_2 nanoarchitecture interfaces can significantly determine the interfacial electron transfer properties by chemical bonding, which is the major factor for enhanced photocatalytic activity, and has not been reported yet. Such chemical bonding interfaces between GNS with TiO_2 shell layer in the GNS-V_2O_5/TiO_2 core/shell nanoarchitecture are expected to increase the surface area and also shorten the diffusion length of photogenerated charge carriers, thus facilitating fast electron transfer across the heterojunction interface. However, the fabrications of free-standing chemically bonded GNS-V_2O_5/TiO_2 core/shell nanoarchitecture are still a challenging task for photocatalytic applications.[19-20] However, it has been rarely reported that the chemical bonding plays an important role in the interfacial charge transfer and enhanced photocatalytic performance.[20-21] Our earlier work in relation to chemical bonding between GNS-TiO_2 and GNS-ZnO nanostructure photocatalysts revealed the formation of the interfaces that contributed much towards photocatalytic performance.[21]

Herein, we demonstrate the fabrication of GNS-V_2O_5/TiO_2 core/shell nanoarchitecture with a chemical bonding interface between C-Ti, prepared by facile hydrothermal method followed by sol-gel techniques. X-ray photoelectron spectroscopy (XPS) analysis confirmed the existence of a C-Ti bonding in the GNS-V_2O_5/TiO_2 hybrid nanoarchitectures. It is proposed that the chemically bonded interfacial charge transfer can provide a good spatial condition for charge transport from GNS to semiconductors and also inhibit the electron-hole recombination rate, confirmed by UPS and PL analysis, respectively. The new nanoarchitecture with a wide light-harvesting capacity and the core/shell heterojunction make it to be an excellent candidate for the degradation of acridine orange dye with enhanced photostability and photocatalytic efficiency.

2. Experimental Section

2.1. Chemicals

All the chemicals used in this work were of analytical grade and used without any further purification. Graphite (325 mesh, Alfa Aesar), potassium permanganate (Sigma-Aldrich), hydrogen peroxide (30 wt%, Sigma-Aldrich), sulfuric acid (Rankem Chemicals), hydrochloric acid (Rankem Chemicals), ammonium meta-vanadate (S-d Fine Chemicals), titanium tetra-isopropoxide (TTIP, Spectrochem), glacial acetic acid (Fischer Chemicals), and AO dye (Fischer Chemicals).

2.2. Synthesis of V_2O_5 nanorods

Vanadium pentaoxide was synthesized from hydrothermal treatment of ammonium meta-vanadate precursor. In a typical synthesis process, 2 mol% of ammonium meta vanadate was dissolved in 50 mL of double distilled water and the solution was stirred until the color changed to yellow. With the above obtained solution, 0.5 mL of HCl was added drop wise and the color of the solution changed to orange and then finally became deep red. The saturated solution was further transferred to 100 mL capacity Teflon-lined stainless steel autoclave. The container was closed tightly and kept in an oven at a temperature of 150°C for 6 hours. The final precipitate was washed and dried in a vacuum oven at 80°C.

2.3. Synthesis of TiO_2 nanogel

In a typical experimental process, 2 mol% (100 mL) of TTIP was used as a metal precursor and glacial acetic acid (10 mL) as a reducing solvent. Both the chemicals were mixed and stirred for 2 hours and then the solution was sonicated for 30 minutes to get a colorless solution. Ultrasonicate the obtained solution for 30 minutes to form a uniform TiO_2 nanogel.

2.4. Synthesis of V_2O_5/TiO_2 core/shell nanorods

We developed a three-step wet chemical approach to fabricate the one-dimensional V_2O_5/TiO_2 core/shell nanostructures without use of any templates. In the first two steps, as-prepared V_2O_5 nanorods were ultrasonically dispersed in 100 mL of distilled water. The shell material TiO_2 nanogel was added on the above synthesized V_2O_5 nanorod dispersions. Nanogel of TiO_2 shell is chemically unstable in the neutral pH-range and therefore it easily aggregates as separate nanomaterials. However, the instability can be controlled by adding HCl to make the pH value of 3, which leads to change in the surface potential of the individual nanomaterials. Then the differences in surface charges are associated with pH that helps to produce a uniform coating of colloidal TiO_2 layer on the V_2O_5 nanorod surfaces by electrostatic attraction. Then the suspension was aged at ambient temperature for 2 hours and finally, the obtained suspension was dried isothermally at 80°C for 12 hours in a vacuum oven. Then, the final product was transferred into the furnace at various temperatures for 2 hours to crystallize the materials.

2.5. Synthesis of GNS decorated with V_2O_5/TiO_2 core/shell nanorods

The synthesis procedure is schematically illustrated in the Fig. 1. GNS was synthesized using modified Hummer's method.[22]

RSC Advances Accepted Manuscript

This journal is © The Royal Society of Chemistry 2012

The obtained GNS (100 mg) was dispersed in double distilled water (100 mL) using ultrasonicator to form a colloidal suspension. The GNS solution was added to a V_2O_5/TiO_2 nanorod suspension, 18 mL of hydrazine hydrate was then added to the resulting solution and the solution was heated to 90°C for 12 hours. The obtained precipitate was separated by centrifugation and subsequent washing with ethanol. The resulting product was dried in a vacuum oven at 100°C for 24 hours to get a GNS-V_2O_5/TiO_2 nanoarchitecture.

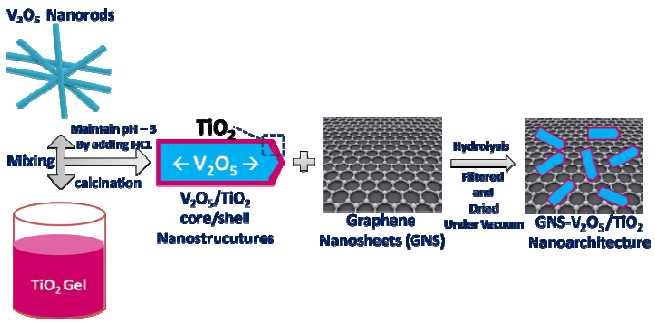

Fig. 1 The schematic illustration of a three-step wet chemical growth process for the formation of GNS-V_2O_5/TiO_2 Nanoarchitecture.

2.6. Instrumentations

The surface potential measurement was analyzed using Malvern Zetasizer Nano ZS90 model, Zeta potential analyzer with 50mW at 532 nm laser source. X-ray diffraction (XRD) data were collected with a PANalytical X-Ray diffractometer using Cu Kα (λ = 1.54 Å) radiation. The samples were scanned in the 2θ range of 10° to 80°. All of the peaks were assigned and compared with the database published by the Joint Committee on Powder Diffraction Standards (JCPDS). XPS measurements were obtained using ESCA+, Omicron Nanotechnology ESCA probe spectrometer with monochromatized Al Kα X-rays (energy: 1486.6 eV). The X-ray power applied was 300 W. The pass energy was 50 eV for survey scans and 20 eV for specific regions. Sample solution was spotted on a molybdenum sample plate and dried in vacuum. Spectra in the required binding energy range were collected, and an average spectrum was taken. Each spectrum was confirmed after scanning eight times for confirmation (except survey scan, which was scanned only once). While taking the spectra, the scan steps per second was maintained as same for all of the narrow scans. Beam-induced damage of the sample was reduced by adjusting the X-ray flux. The base pressure of the instrument was 5.0×10^{-10} mB. The binding energy was calibrated with respect to the adventitious C 1s feature at 284.6 eV. Most of the spectra were deconvoluted to their component peaks, using the software CASA-XPS. High-resolution scanning transmission electron microscopy (HRSTEM) of the samples was carried out using a FEI Tecnai G2 S-twin instrument with a UHR pole piece. HRSTEM samples were prepared by drop-casting two or three drops of sample-dispersed ethanol solution to carbon-coated copper grids and allowed to dry at room temperature overnight. All measurements were done at 300 kV accelerating voltage. UPS measurements were obtained using ESCA+, Omicron nanotechnology equipped with VUV source HIS 13 gas discharge light source for the production of VUV light below 10^{-9} mbar vacuum conditions. It was operated with He I mode emission line at 21.2 eV (584 nm) used for this analysis. The photoluminescence (PL) spectrum was recorded by Perkin Elmer MPF-44B equipment under (325 nm) excitation.

2.7. Photocatalytic activity

A mutagenic organic dye AO was used to evaluate the photocatalytic activity of the fabricated nanoarchitectures. A photocatalyst (10 mg) was dispersed with three different AO dye concentrations, 2.5×10^{-5} M, 3.0×10^{-5} M, and 3.5×10^{-5} M individually in 50 mL of aqueous solution using ultrasonicator. Before exposure to illumination, the suspensions were stirred in the dark for 30 minutes to ensure the establishment of adsorption/desorption equilibrium of AO on the sample surfaces. Consequently, the suspension was irradiated with direct sunlight and this was carried out for all the experiments under similar conditions on sunny days of April 2014 in Chennai city (geographical location 13.04° N and 80.17° E on the southern-east coast of India), between 12:00 p.m. and 3:00 p.m. (outside temperature, 29°C to 31°C). The measured illuminance power of the direct sunlight at the given interval of time was around 110000 lux to 120000 lux obtained by using Digital illuminance meter (TES Electrical Electronic Corp. Taiwan). At a given time interval of irradiation, 5 mL of the suspension was withdrawn and subsequently centrifuged at a rate of 3000 rpm for 5 minutes. UV–Vis absorption spectra of the supernatant were then measured using a UV–visible spectrophotometer.

3. Results and Discussion

3.1. Surface potential analysis

Zeta potential measurement was performed for V_2O_5 nanorods and TiO_2 nanogel in order to analyze the surface charge of the as-prepared nanomaterials. Figure 2 shows the obtained Zeta potential plot as a function of pH. The obtained potential was found to decrease with a decrease of pH, as is expected for surface coating properties and also the core/shell formation process. The difference in surface potential is related to the variation in pH value of the materials.

RSC Advances Accepted Manuscript

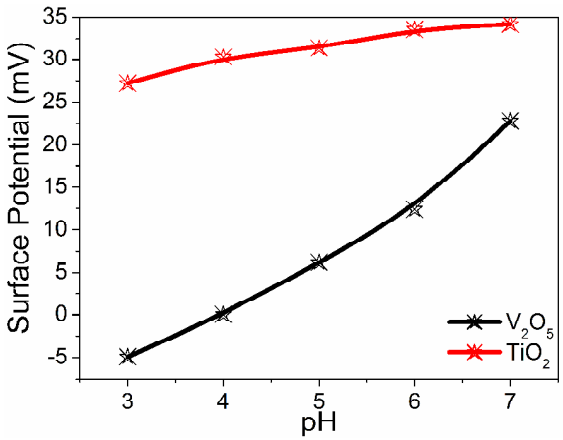

Fig. 2 Surface potential plot as a function of pH for V_2O_5 and TiO_2 nanomaterials.

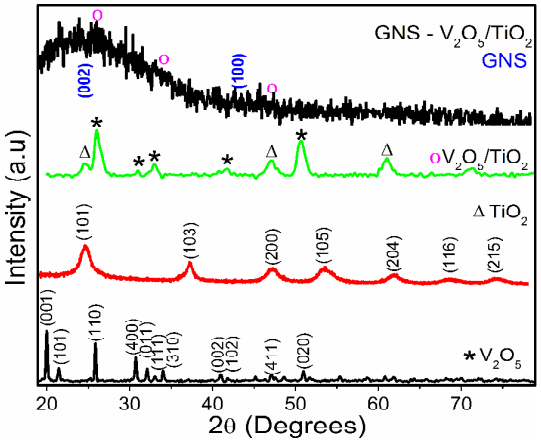

Fig. 3 XRD patterns of V_2O_5, TiO_2, V_2O_5/TiO_2, and GNS-V_2O_5/TiO_2 nanoarchitectures.

On reducing pH of pure V_2O_5 and TiO_2 by adding HCl (pH-3), the surface potential shows -5.02 mV and +27.2 mV, respectively. The TiO_2 nanogel was coated on the V_2O_5 nanorods surface by electrostatic attraction. Since the entire TiO_2 shell nanolayer has higher surface charges than the core V_2O_5 nanorods, it could be a reason to believe that the nanoshells have encapsulated on the V_2O_5 surfaces.[23-24]

3.2. Structural analysis

The XRD was used to analyze the crystallographic structures of as-synthesized V_2O_5, TiO_2, $V2O_5/TiO_2$ core/shell nanorods, and GNS-V_2O_5/TiO_2 nanoarchitectures, as shown in Fig. 3. The XRD pattern clearly shows that the crystalline phase of orthorhombic V_2O_5 and anatase phase of TiO_2 coexist in the V_2O_5/TiO_2 core/shell nanorods. All diffraction peaks of pure V_2O_5 and TiO_2 can be seen (in Fig. 3), in good agreement with the reported data (JCPDS card No. 89-0612) and (JCPDS card No. 21-1272), respectively. In GNS-V_2O_5/TiO_2 sample, GNS show a broad peak at 25.7 and 41.16 degrees, corresponding to the (002) and (100) reflections. It is evident that the graphene oxide is considerably reduced to graphene nanomaterials.[25] Very low quantity of V_2O_5/TiO_2 core/shell nanorods were chemically bonded on the GNS surfaces that can be clearly compared and analyzed with individual nanomaterials. However, the existence and chemical bonding nature of V_2O_5/TiO_2 with GNS can be obviously elucidated by XPS analysis, as discussed in the next section.

3.3. Chemical bonding analysis

To study the chemical bonding interaction between V_2O_5/TiO_2 core/shell nanostructures and GNS-V_2O_5/TiO_2 nanoarchitectures were analyzed by XPS spectra. Figures 4a and 4b exhibits the high-resolution XPS spectra of V 2p and Ti 2p regions for the V_2O_5/TiO_2 core/shell nanostructure sample. The binding energies at 526.8 eV and 519.2 eV are assigned to V $2p_{1/2}$ and V $2p_{3/2}$ spin-orbital splitting in the V^{5+} state and at 460.9 eV and 455.1 eV corresponding to Ti $2p_{1/2}$ and Ti $2p_{3/2}$ that are related to Ti^{4+} oxidation state, respectively. Besides, there is no shift in the binding energies between V_2O_5 and TiO_2 in the V_2O_5/TiO_2 core/shell nanorod structures.[8,14] These results provide the evidence that TiO_2 ions does not enter into the V_2O_5 lattices, it remains together by electrostatic interaction and not a chemical bonding. Furthermore, the deconvoluted peaks centered at the binding energy of 284.6 eV and 286.9 eV were attributed to the C-C and C-O bands (in Fig. 4e), which suggests the presence of only few oxygen-containing functional groups in V_2O_5/TiO_2 core/shell nanorod structures.

Figures 4c and 4d show the high-resolution XPS spectra of V 2p and Ti 2p regions for GNS-V_2O_5/TiO_2 core/shell nanoarchitecture samples. The binding energies at 526.8 eV and 519.2 eV are assigned to V $2p_{1/2}$ and V $2p_{3/2}$ that are related to V^{5+} oxidation state and at 461.2 eV and 455.6 eV corresponding to Ti $2p_{1/2}$ and Ti $2p_{3/2}$ that are related to Ti^{4+} oxidation state, respectively. It indicates that the oxidation state of Ti^{4+} was accredited to the formation of C-Ti bonding due to the small variations in the Ti peak position as compared to V_2O_5/TiO_2 core/shell nanostructure sample.[20]

RSC Advances Accepted Manuscript

This journal is © The Royal Society of Chemistry 2012

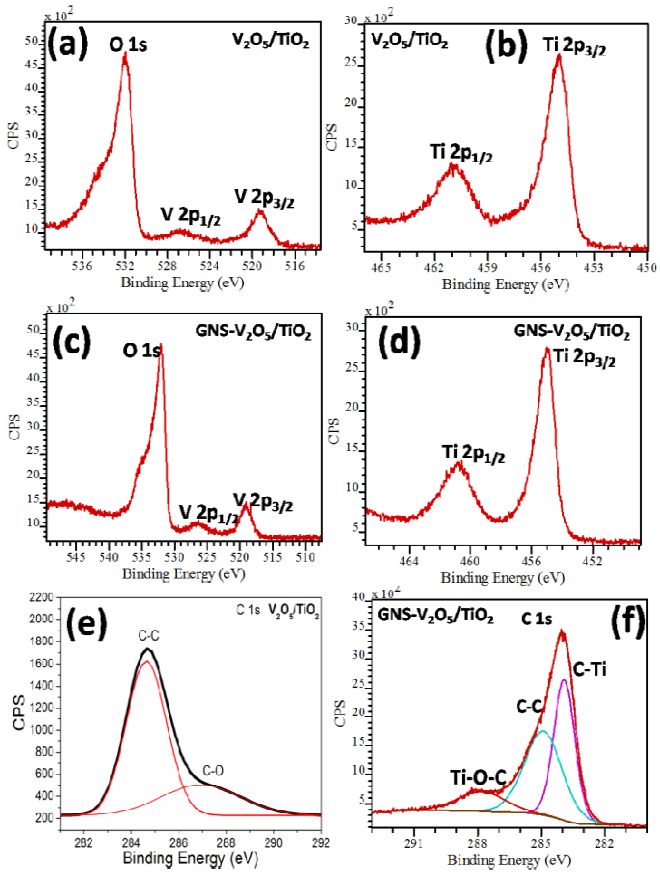

Fig. 4 The V 2p, Ti 2p and C 1s XPS spectra; V_2O_5/TiO_2 core/shell nanorods (a, b and e) and GNS-V_2O_5/TiO_2 core/shell nanoarchitectures (c, d and f).

The C1s graph of GNS-V_2O_5/TiO_2 core/shell nanoarchitecture (in Fig. 4f) can be deconvoluted into three peaks at binding energies of 283.6 eV, 284.6 eV, and 288.4 eV, which are assigned to C-Ti, C-C and Ti-O-C bonding, respectively. The oxygen-containing bond at 283.6 eV on the surface of GNS can act as a bonding site for TiO_2 shell layer. During the reaction process, the oxygen-containing group completely reduced and formed to C-Ti bond, which is present in the shell part of the core/shell nanostructures. In addition, the peak at 286.9 eV disappears, and a characteristic peak emerges at 288.4 eV accredited to Ti–O–C bond was also observed. This shift indicating that the –OH group of TiO_2 possibly interacts with the –COOH group on the surface of GNS during the reaction process.[26-27] These data demonstrated that the C-Ti chemical bonds are present in GNS-V_2O_5/TiO_2 core/shell nanoarchitectures.

3.4. Electron microscopic studies

The HRSTEM images of the as-prepared V_2O_5, TiO_2, V_2O_5/TiO_2 core/shell nanorods, and GNS-V_2O_5/TiO_2 nanoarchitectures are shown in Fig. 5 and 6. The obtained morphologies of the orthorhombic V_2O_5 nanomaterials were uniform nanorods of diameter ranging from 40 nm to 50 nm and the length reaching few micrometers with the lattice distance of 0.43 nm corresponds to (001) plane as observed from the obtained images shown in Fig. 5 (a) and (c). It seems likely that the conditions of this synthesis route are best suited for the homogenous growth of elongated orthorhombic V_2O_5 nanorods. To obtain core/shell nanostructures, TiO_2 nanospheres with average size of 3 nm to 10 nm particles with the measured lattice distance of 0.35 nm corresponds to (101) plane of anatase structure (in Fig. 5 b&d) were coated onto the V_2O_5 nanorods under stimulated reaction medium. Due to the variation in the surface potential of the individual nanomaterials, V_2O_5/TiO_2 core/shell nanorods were formed by electrostatic attraction of the nanomaterials. In Fig. 6a, it is clearly demonstrated that a layer of TiO_2 nanomaterials is uniformly coated on the surface of individual V_2O_5 nanorods to form one-dimensional core/shell nanostructures. The respective inset clearly shows the surface of the V_2O_5 nanorods were completely coated with crystalline TiO_2 nanoshells of diameter of about 15 nm to 20 nm and the core V_2O_5 diameter of about 120 nm to 140 nm.

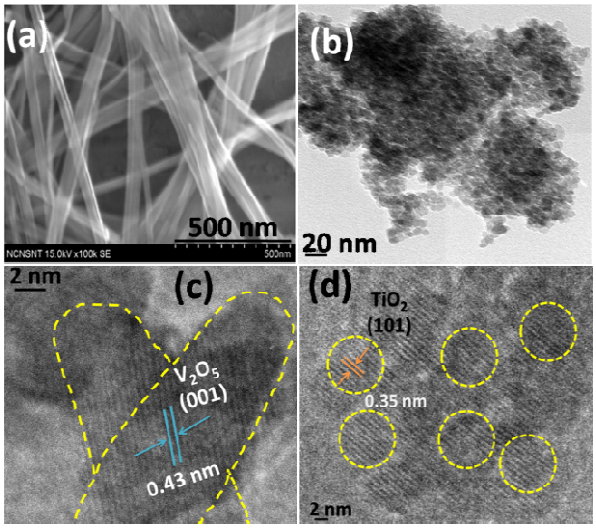

Fig. 5 Electron micrographs of V_2O_5 (a), TiO_2 (b), lattice fringes of V_2O_5 (c) and TiO_2 (d) nanostructures.

Figure 6b shows the formation of GNS as distributed uniformly and indicates its ultrathin thickness. This is evident that the GNS indeed acts as a two-dimensional nanostructure support for the incorporation and growth of homogeneous core/shell nanostructures. After incorporation with V_2O_5/TiO_2 core/shell nanorods, the GNS was decorated by V_2O_5/TiO_2 core/shell nanorods. Because of the chemical bonding and preferential nucleation reaction in the synthesis medium, the surface of the core/shell nanorods were chemically bonded (in Fig. 6c) with the GNS surface. The corresponding inset shows the clear pictorial representation of GNS-V_2O_5/TiO_2 nanoarchitectures. Figure 6d shows the lattice fringe image of the GNS-V_2O_5/TiO_2 interface, where it can be seen that the strong alignment of the two different crystal lattices results in hetero-epitaxial growth of V_2O_5/TiO_2 nanorods on GNS. The measured lattice distance of 0.43 nm corresponds to the (001) plane of orthorhombic V_2O_5. We also observe that the lattice fringes on the edges of the V_2O_5 with the lattice distance of 0.35

RSC Advances Accepted Manuscript

nm corresponds to (101) plane of anatase TiO_2.[14,28] It demonstrates that the exposed facets of TiO_2 were embedded onto the surface of graphene indicating that there was an interaction between Ti atoms with GNS.

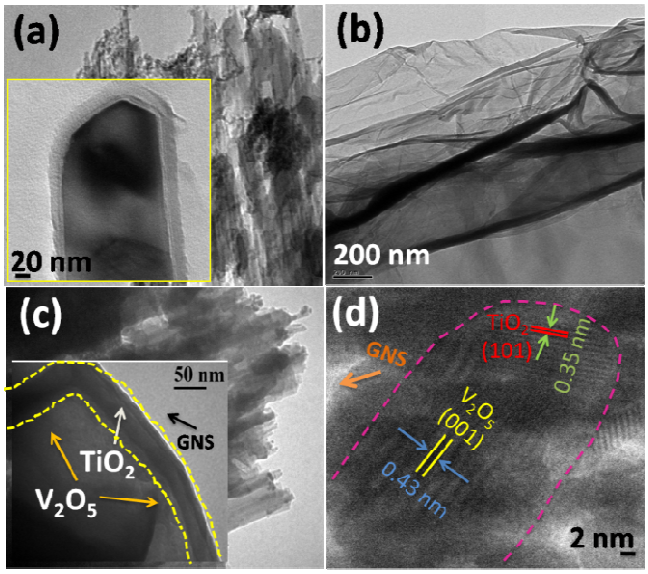

Fig. 6 Electron micrographs of V_2O_5/TiO_2 core/shell (a), GNS (b), GNS-V_2O_5/TiO_2 core/shell (c) and lattice fringes of GNS-V_2O_5/TiO_2 core/shell nanoarchitectures.

3.5. Photocatalytic degradation of AO dye under direct sunlight irradiation

The photocatalytic activity of the as-prepared V_2O_5, V_2O_5/TiO_2, and GNS-V_2O_5/TiO_2 nanoarchitectures were examined by monitoring the degradation of mutagenic organic pollutants (AO dye) under direct sunlight irradiation. The change in absorption spectra of AO aqueous solution showed the changes of its concentration. The initial concentration (C_0), the residual concentration (C), and the degradation rate (D%), is illustrated by the mathematical expression as follows:

$$D\% = (C_0 - C/C_0) \times 100\% \quad (1)$$

Figure 7a showed the AO degradation plot versus time for V_2O_5, V_2O_5/TiO_2, and GNS-V_2O_5/TiO_2 nanoarchitecture photocatalysts, respectively. C/C_0 spectra indicate that the 2.5×10^{-5} M concentration of AO dye was decomposed of about 40% for pure V_2O_5 nanorods within 60 minutes, 95% for V_2O_5/TiO_2 core/shell nanorods within 60 minutes and 100% for GNS-V_2O_5/TiO_2 nanoarchitectures within 20 minutes (in Fig. 7b) under direct sunlight irradiation. GNS-V_2O_5/TiO_2 nanoarchitectures exhibited higher photocatalytic efficiency than that of the pure and core/shell nanomaterials. This result demonstrates that GNS enhances the photocatalytic activity of V_2O_5/TiO_2 core/shell nanorods under direct sunlight irradiation. The dye suspension with the photocatalyst (GNS-V_2O_5/TiO_2) was kept in dark conditions for 30 minutes to ensure the establishment of adsorption/desorption equilibrium of AO on the sample surfaces (refer Fig. 7a). With the help of GNS, adsorption of dyes is gradually increased by π–π bonding interactions with the aromatic regions of GNS. Hence, GNS showed the better adsorption of AO than that of pure and core/shell metal oxide semiconductors mainly due to its great π-conjugated system and two-dimensional honey comb structure.[29-30] Chemically combining the selective metal oxide heterostructures onto GNS surfaces led to faster organic dye absorption as well as drastic photodegradation under sunlight irradiation.

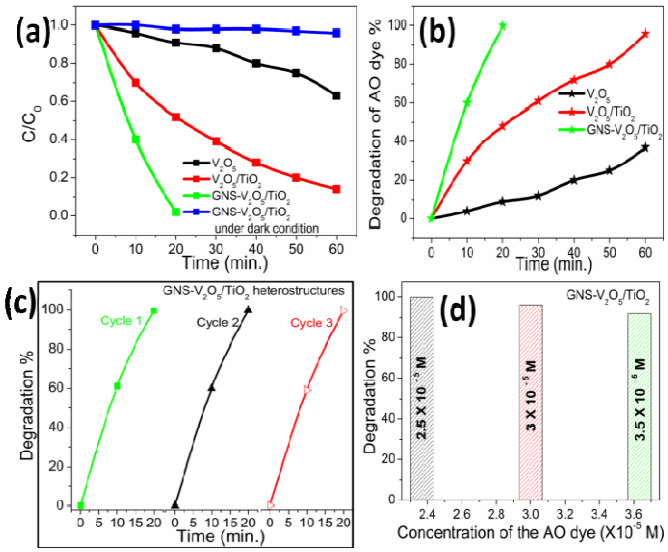

Fig. 7 Time-dependent photocatalytic activity C/C_0 plot (a), degradation percentage of AO in the presence of obtained hybrid photocatalysts (b), stability and reusability experiment (c), and concentration-dependent AO dye degradation under direct sunlight irradiation using GNS-V_2O_5/TiO_2 hybrid nanoarchitecture photocatalysts.

Moreover, the stability of the hybrid nanoarchitecture photocatalysts was examined by three experimental cycles, which were very crucial for the photocatalyst to be applied in environmental technology. Figures 7c and d illustrate that the photocatalytic degradation process of AO over GNS-V_2O_5/TiO_2 hybrid nanoarchitecture photocatalyst under sunlight irradiation was effectual. More importantly, by increasing the AO dye concentrations like 2.5×10^{-5} M, 3.0×10^{-5} M, and 3.5×10^{-5} M, and it was indicated that the GNS-V_2O_5/TiO_2 hybrid nanoarchitecture photocatalyst could easily degrade the AO dye within 20 minutes of irradiation under direct sunlight and can be separated and reused by centrifugation. It would be significantly promote their practical application to remove the harmful mutagenic organic pollutants from wastewater.

3.6. Mechanism of enhanced photocatalytic activity under sunlight

From the above characterization analysis, the proposed mechanism of the efficient photocatalytic activity toward the degradation of organic pollutant under sunlight could be accredited mainly due to interfacial charge transfer of GNS by chemical bonding between GNS and TiO_2 shell in V_2O_5/TiO_2 core/shell nanorods. Interfacial transfer of charge carrier plays an important role in photocatalytic processes. Once the photo-excitation induces a transition of electrons from the valence band to conduction band, leaving an equal number of holes at

RSC Advances Accepted Manuscript

This journal is © The Royal Society of Chemistry 2012

valence band, the excited electrons and holes migrate to the surface. Most of the excited electron–hole pairs recombine and dissipate the energy in the form of heat or emitted light. To avoid the recombination rate of electron–hole pairs, some fast electron mobility co-catalysts (GNS) with heterostructured core/shell metal oxides are incorporated.[21] The formation of hetero-junctions between the core/shell metal oxides and the co-catalyst generate a local electric field that separates the electron–hole pairs completely and induces spacial conduction as well as faster interfacial charge transfer.[31-33] In addition, the interaction between metal oxide semiconductors and co-catalysts (GNS) exhibit better conductivity and higher catalytic activity than the host.

From the above context, heterostructured core/shell metal oxide semiconductors, such as V_2O_5/TiO_2 was electrostatically bonded together and decorated onto the GNS surfaces with chemical bonding interaction that can effectively facilitate the interfacial electron transfer and electron−hole separation. During photocatalytic process, the conduction band and valence band of V_2O_5 lie above the energy band of TiO_2. This results in the gathering of a large number of electrons in the conduction band of TiO_2 and holes in the valence band of V_2O_5. So the photogenerated electrons and holes can be separated efficiently at the interface. The oxygen molecules adsorbed on the surface of the photocatalysts could react with the free electrons. For the transfer of these electrons from one semiconductor grain to another, it should get through the potential barrier and this limits the electron mobility. If the semiconductor core/shell structures were chemically bonded onto the GNS surface, they can obviously decrease the potential barrier and increase the band gap energy of the GNS. Such chemical bonding could provide an efficient charge carrier transport and good spatial condition from semiconductors to GNS via the heterojunction.

The electron transfer mechanism (in Fig. 8) of GNS-V_2O_5/TiO_2 nanoarchitectures can be expressed by the following equation:

$$V_2O_5/TiO_2 + h\nu \rightarrow e^-(CB, TiO_2) + h^+(VB, V_2O_5) \quad (2)$$

$$GNS + e^-(CB, TiO_2) \rightarrow e^-(GNS) + TiO_2 \quad (3)$$

$$GNS + e^-(AO) \rightarrow e^-(GNS) + AO \quad (4)$$

$$H_2O + h^+(VB, V_2O_5) \rightarrow \bullet OH + H^+ \quad (5)$$

$$AO\ (ad) + \bullet OH \rightarrow CO_2 + H_2O \quad (6)$$

On the other hand, photogenerated electrons cannot flow directly from AO to V_2O_5/TiO_2 metal oxide core/shell nanostructures, since there was a mismatch in their energy levels. A photo-excited electron from AO flows into CB of TiO_2 shell in the V_2O_5/TiO_2 core/shell nanostructures via GNS, where radical species are generated. Usually pollutants are aromatic compounds that create π–π stacking with GNS, and subsequently there is a creation of oxidants and then the reduction of radicals generate the reactive species and degrade the pollutants. Therefore, the photodegradation is enhanced by chemical bonding between core/shell nanostructures with GNS surfaces and also π–π interactions.[34-37] Moreover, interfacial charge transfer, high electron mobility, and enhanced efficiency in charge separation improve the higher photocatalytic activity.

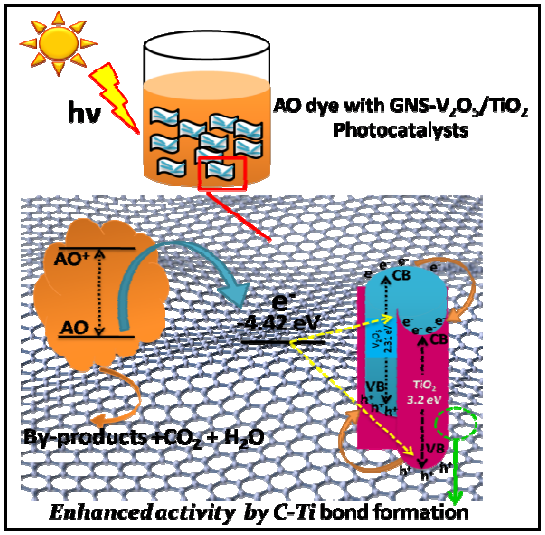

Fig. 8 Schematically illustrate the charge transfer mechanism for enhanced photocatalytic activity.

3.7. Band alignment and work function analysis

The most important requirement for a heterostructures photocatalyst is alignment of energy levels of the semiconductors. Here, we applied the UPS technique to measure the valence band edge of the GNS-V_2O_5/TiO_2 with respect to pure and core/shell nanostructures present in Fig. 9. Based on the upper (E_1) and lower (E_2) emission onset energy levels of the secondary photoelectrons from the samples,[38] we estimated the work function using the following equation:

$$\phi = h\nu - (E_1 - E_2) \quad (7)$$

For V_2O_5, V_2O_5/TiO_2, and GNS-V_2O_5/TiO_2 nanoarchitectures, the values of E_1 were 15.6 eV, 15.7 eV, and 15.9 eV, respectively, and those of E_2 were 2.6 eV, 2.6 eV, and 2.6 eV, respectively. Therefore, the work functions (in Fig. 10) for V_2O_5, V_2O_5/TiO_2, and GNS-V_2O_5/TiO_2 nanoarchitectures were 8.21 eV, 8.11 eV, and 7.91 eV, respectively. The decreases in the work functions are mainly accredited to the strong interfacial charge transfer from GNS to TiO_2 and V_2O_5 to create interface dipoles originating from exchange effects.[39-42] These interfacial charge transfer effects will increases the photocatalytic efficiency. The ionization energy of the nanoarchitecture photocatalysts were calculated using the equation,

$$E_{ion} = WF + VBM \quad (8)$$

The E_{ion} (in Fig. 10) decreases from 10.81 eV (V_2O_5) to 10.71 eV (V_2O_5/TiO_2), and 10.51 eV (GNS-V_2O_5/TiO_2) demonstrating the good electron transporting properties between the heterostructure semiconductors and GNS.[44] Therefore, GNS is a promising candidate for enhancing the photocatalytic activity of the semiconductors, inhibiting the recombination rate, and accelerating the interfacial charge transfer process.

RSC Advances Accepted Manuscript

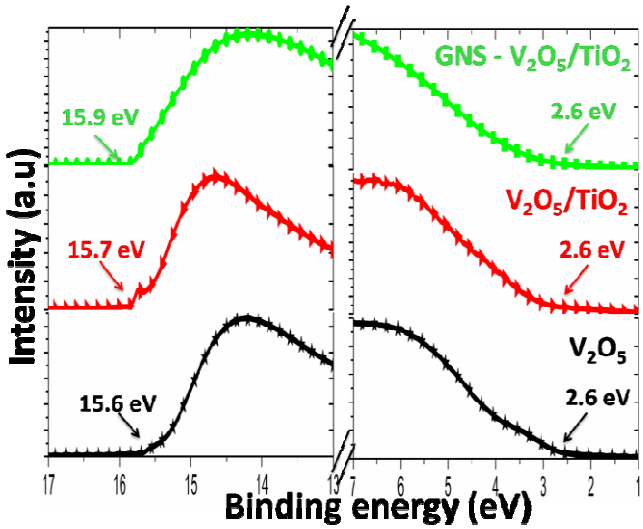

Fig. 9 The UPS spectra of the as-prepared V_2O_5, V_2O_5/TiO_2, and GNS-V_2O_5/TiO_2 nanoarchitectures.

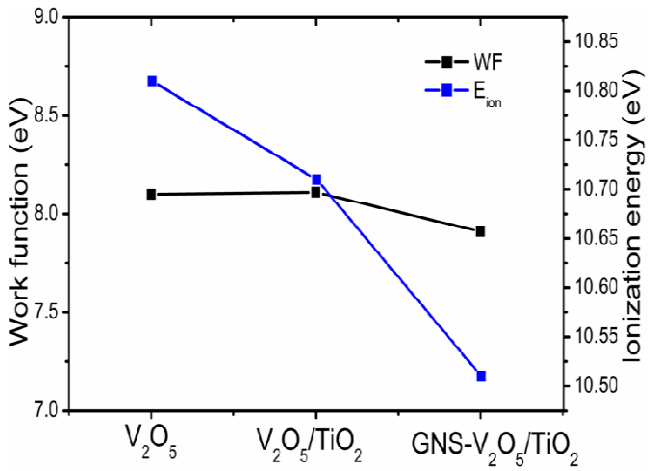

Fig. 10 Work function (WF) and ionization energy (E_{ion}) plot for the V_2O_5, V_2O_5/TiO_2, and GNS-V_2O_5/TiO_2 nanoarchitectures.

3.8 Photoluminescence analysis

The photogenerated electron–hole pair recombination kinetics is examined to be an important factor that affects the photocatalytic efficiency of a photocatalyst. The electron–hole pair recombination rate can be experimentally determined by PL emission spectra. Decrease in the PL emission intensity indicates the better charge separation efficiency. Figure 11 shows the PL emission spectra of V_2O_5, V_2O_5/TiO_2, and GNS-V_2O_5/TiO_2 nanoarchitectures. It is evident that the two prominent peaks at 401 nm and 427 nm in the visible region have been observed for V_2O_5 nanorods. This suggests that the presence of defect related emission; in particular oxygen-ion vacancies arbitrate the recombination of photo induced electron–hole pairs in the semiconductor nanorods.[8] The PL spectra of the V_2O_5/TiO_2 core/shell nanorods compared with the pure V_2O_5 nanorods, the intensity of the V_2O_5 peaks decreases significantly due to the presence of TiO_2 shell layer. It is evident that there is a heterojunction between the semiconductors that certainly reduces the defect during core/shell formation process.

For comparison, chemically bonded GNS-V_2O_5/TiO_2 nanoarchitectures were analyzed with PL emission spectra. The emission intensity decreased largely, suggesting that the bonding with GNS could quench the fluorescence from the semiconductor nanomaterials.[21] The quenching mechanism of the PL spectra may be due to the interfacial charge transfers from the excited semiconductor core/shell nanostructures. It may be possible to increase the rate of charge transfer between the semiconductors and GNS due to chemical bonding. As a result, GNS is a promising candidate for efficiently increase the photocatalytic activity in terms of prolonging the electron–hole pair lifetime, which inhibits the recombination rate and accelerates the interfacial charge transfer process.

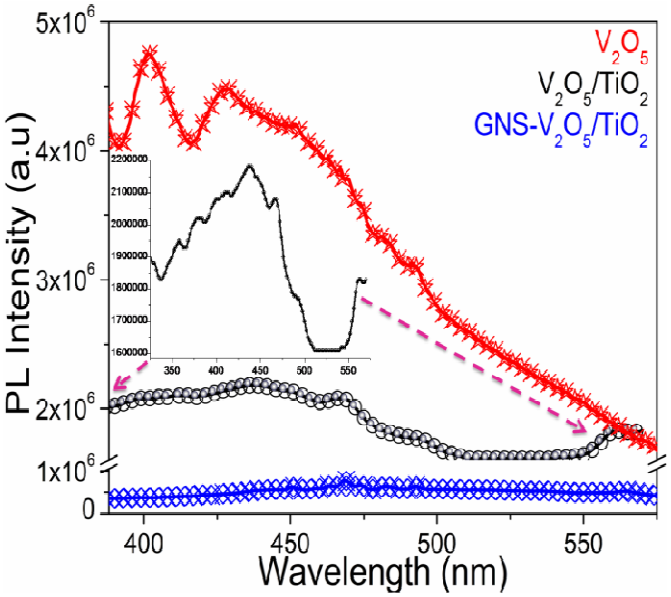

Fig. 11 Room temperature PL spectra of the V_2O_5, V_2O_5/TiO_2 core/shell and GNS–V_2O_5/TiO_2 core/shell nanoarchitectures.

4. Conclusions

In summary, GNS-V_2O_5/TiO_2 nanoarchitectures have been successfully synthesized by a facile hydrothermal process followed by a sol-gel technique. Such nanoarchitecture is made up of V_2O_5/TiO_2 core-shell nanorods anchored on GNS with close interfacial contacts. Further characterization results indicate that the TiO_2 shells in the V_2O_5/TiO_2 core/shell nanorods were chemically bonding with the GNS which is confirmed by the formation of the C−Ti bond using XPS. The chemically bonded nanoarchitecture GNS-V_2O_5/TiO_2 exhibits higher photocatalytic activity than the pure materials. On the basis of the work function and ionization energy value results, this enhancement can be explained by the interfacial charge transfer effect, which could provide a good spatial condition for charge transport from GNS to semiconductors via the chemical bonding, and thus lead to higher photocatalytic activity.

RSC Advances Accepted Manuscript

This journal is © The Royal Society of Chemistry 2012

Acknowledgements

R. Ajay Rakkesh gratefully acknowledge the University of Madras for providing NCNSNT fellowship (C2/AL/2011/388) supported by MHRD, India to carry out the research work. D. Durgalakshmi gratefully acknowledges Lady Tata Memorial trust, Mumbai for awarding Junior and Senior Fellowship to support the research work. We thank Dr. S. Ramaprabhu, Head, Alternative energy and Nanotechnology Laboratory, Department of Physics, IIT Madras for availing the BET facility.

Notes and references

National Centre for Nanoscience and Nanotechnology, University of Madras, Guindy campus, Chennai 600025, India.
Fax: 044-22352494/22353309; Tel: 044-22202749
*E-mail: balasuga@yahoo.com

Electronic Supplementary Information (ESI) available: Photocatalytic activity of Methylene blue dye using obtained hybrid photocatalysts, N_2 adsorption – desorption results of V_2O_5, V_2O_5/TiO_2 and GNS- V_2O_5/TiO_2 nanoarchitectures and HRSTEM fringes pattern of V_2O_5/TiO_2 core/shell nanostructures. See DOI: 10.1039/b000000x/

1. R. Ostermann, D. Li, Y. Yin, J. T. Mccann, and Y. Xia, *Nano Lett*, 2006, **6**, 1297.
2. P. M. Rao, L. Cai, C. Liu, I. S. Cho, C. H. Lee, J. M. Weisse, P. Yang, and X. Zheng, *Nano Lett*, 2014, **14**, 1099.
3. G. Lia and Z. Tang, *Nanoscale*, 2014, **6**, 3995.
4. L. Xu, M. L. Yin and S. Liu, *Sci. Rep.*, 2014, **4**, 6745.
5. Q. Zhang, I. Lee, J. B. Joo, F. Zaera, And Y. Yin, *Accounts Chem Res*, 2013, **46**, 1816.
6. J. Su, Y. Zhang, S. Xu, S. Wang, H. Ding, S. Pan, G. Wang, G. Li and H. Zhao, *Nanoscale*, 2014, **6**, 5181.
7. Y. Liu, L. Zhao, M. Li and L. Guo, *Nanoscale*, 2014, **6**, 7397.
8. Y. Wang, Y R Su, L Qiao, L X Liu, Q Su, C. Q. Zhu and X. Q. Liu, *Nanotechnology*, 2011, **22**, 225702.
9. A. Fujishima and K. Honda, *Nature,* 1972, **238**, 37.
10. A. Mills and S.L. Hunte, *J. Photochem. Photobiol. A*, 1997, **108**, 1.
11. W. Y. Choi, A. Termin and M. R. Hoffmann, *Angew. Chem., Int. Ed. Engl.,* 1994, **33**, 1091.
12. J. Moon, C. Y. Yun, K. W. Chung, M. S. Kang and J. Yi, *Catal.Today*, 2003, **87**, 77.
13. Y. Wang, J. Zhang, L. Liu, C. Zhu, X. Liu, Q. Su, *Mater. Lett*., 2012, **75**, 95.
14. (a) S. Martha, D. P. Das, N. Biswal and K. M. Parida, *J. Mater. Chem.,* 2012, **22**, 10695; (b) Z. Liu, Y. Li, C. Liu, J. Ya, L. E, W. Zhao, D. Zhao, and Li An, *ACS Appl. Mater. Interfaces*, 2011, **3**, 1721; (c) K. Lee and G. Cao, *J. Phys. Chem. B*, 2005, **109**, 11880; (d) Z. Liu, K. Guo, J. Han, Y. Li, T. Cui, B. Wang, J. Ya, and C. Zhou, *small*, 2014, **10**, 3153; (e) X. Wang, G. Liu, G. Q. Lu, and H. M. Cheng, *Int J Hydrogen Energy*, 2010, **35**, 8199.
15. Y. Zhang, Y. W. Tan, H. L. Stormer, P. Kim, *Nature*, 2005, **438**, 201.
16. A. K. Geim, K. S. Novoselov, *Nat. Mater*., 2007, **6**, 183.
17. G. Williams, B. Seger and P. V. Kamat, *ACS Nano*, 2008, **2**, 1487.
18. P. Wang, Y. Zhai, D. Wang and S. Dong, *Nanoscale*, 2011, **3**, 1640.
19. N. Li, M. Cao and C. Hu, *Nanoscale*, 2012, **4**, 6205.
20. Q. Huang, S. Tian, D. Zeng, X. Wang, W. Song, Y. Li, W. Xiao and C. Xie, *ACS Catal*., 2013, **3**, 1477.
21. R. Ajay Rakkesh, D. Durgalakshmi and S. Balakumar, *J. Mater. Chem. C*, 2014, **2**, 6827.
22. J. Liqiang, Q. Yichuhn, W. Baiqi, L. Shudan, J. Baojiang, Y. Libin, F. Wei, F. Honggang and S. Jiazhong, *Sol. Energy Mater. Sol. Cells*, 2006, **90**, 1773.
23. P. Wilhelm and D. Stephan, *J. Colloid Interf. Sci.,*2006, **293**, 88.
24. R. Ajay Rakkesh and S. Balakumar, *J. Nanosci. Nanotechnol*., 2013, **13**, 370.
25. J. Liu, H. Bai, Y. Wang, Z. Liu, X. Zhang and D. D. Sun, *Adv. Funct. Mater*., 2010, **20**, 4175.
26. J. H. Park, S. Kim, A.J. Bard, *Nano Lett*., 2006, **6**, 24.
27. Y. Wang, H. Li, L. Ji, X. Liu,Y. Wu, Y. Lv, Y. Fu,H. Zhou, J. Chen, *J. Phys. D: Appl.Phys*., 2012, **45**, 295301.
28. K. V. R. Chary, G. Kishan, T. Bhaskar and C. Sivaraj, *J. Phys.Chem. B*, 1998, **102**, 6792.
29. Z. T. Hua, J. Liub, X. Yana, W. D. Oha, T. T. Lim, *Chem. Eng. J*., 2015, **262**, 1022.
30. Y. J Wang, R. Shi, J. Lin and Y. F. Zhu, *Energy Environ. Sci*., 2011, **4**, 2922.
31. A. Cao, Z. Liu, S. Chu, M. Wu, Z. Ye, Z. Cai, Y. Chang, S. Wang, Q. Gong and Y. Liu, *Adv. Mater*., 2010, **22**, 103.
32. Y. Liang, H. Wang, H. Sanchez Casalongue, Z. Chen and H. Dai, *Nano Res*., 2010, **3**, 701.
33. W. Tu, Y. Zhou and Z. Zou, *Adv. Funct. Mater*., 2013, **23**, 4996.
34. Y. Bu, Z. Chen, W. Li, and B. Hou, *ACS Appl. Mater. Interfaces*, 2013, **5**, 12361.
35. D. Chen, H. Zhang, Y. Liu and J. Li, *Energy Environ. Sci*., 2013, **6**, 1362-1387.
36. N. Zhang, Y. Zhang and Y. J. Xu, *Nanoscale*, 2012, **4**, 5792.
37. H. Gao, X. Li, J. Lv, and G. Liu, *J. Phys. Chem. C*, 2013, **117**, 16022.
38. J. H. Huang, T.Y. Huang, H.Y. Wei, K. C. Hobc and C. W. Chu, *RSC Advances*, 2012, **2**, 7487.
39. P. S. Bagus, V. Staemmler and C. Woll, *Phys. Rev. Lett*., 2002, **89**, 096104.
40. H. O. Seo, S.Y. Park, W. H. Shim, K.D. Kim, K. H. Lee, M. Y. Jo, J. H. Kim, E. Lee, D.W. Kim, Y. D. Kim and D. C. Lim, *J. Phys. Chem. C*, 2011, **115**, 21517.
41. J. H. Lee, J. H. Shin, J. Y. Song, W. Wang, R. Schlaf, K. J. Kim and Y. Yi, *J. Phys. Chem. C*, 2012, **116**, 26342.
42. K. Yuan, L. Chen, F. Lia and Y. Chen, *Mater. Chem.C*, 2014, **2**, 1018.

RSC Advances Accepted Manuscript